Comparison of NACA 0012 and KFm-4 wing profiles for high subsonic speed unmanned aerial vehicles

Muktedir Gözüm [*1] and Cevat Özarpa [2]

[1]*Ankara Medipol University Health Services Vocational School of Higher Education, Biomedical Device Technology Department, Ankara, Türkiye*
[2]*Ankara Medipol University Engineering Faculty Biomedical Engineering Department, Ankara, Türkiye*

Article Info	Abstract
	KFm airfoil, attracts attention among radio-controlled aircraft enthusiasts due to its simplicity of construction. It was not preferred in manned aircraft due to its poor lift-to-drag ratio performance in wind tunnel tests. In this article, by comparing it with the NACA0012 profile, which is generally preferred at high subsonic speeds, the consequences of choosing the KFm-4 wing profile over the NACA0012 profile due to its ease of production, and what advantages and disadvantages it has. The comparison; While increasing the speed of high-speed unmanned aerial vehicles, it will be important to fly more stable, have better maneuverability, reduce the drag force and delay separation. The calculations were obtained by performing computational fluid dynamics analysis in 2 dimensions. Analysis was conducted under conditions of a low Reynolds number, with a consistent velocity at Mach 0.6 and a zero-degree angle of attack. To validate the precision of the outcomes, a series of tests were executed, involving variations in grid size or node configurations. With the increase in the number of nodes, the lift coefficient exhibited a rising trend; however, upon reaching 305100 nodes, further increase in nodes did not lead to any significant change in the lift coefficient. As a result, a lift coefficient value of 0.1010 was obtained for the NACA 0012 profile, while a lift coefficient value of 0.0720 was obtained for the KFm-4 profile. Thus, it was concluded that it would be more appropriate to use the NACA 0012 profile in high-speed unmanned aerial vehicles.

1. Introduction

Unmanned aerial vehicles are very important today, both civilian and military, especially in missions where the risk of losing an aircraft is high. In this case, the aircraft must aerodynamically perform its duty stably at both low and high subsonic speeds (<980 kmh=609 mph=0.8 Mach). For this, the wing profile must be selected correctly so that the aircraft can fly stably even at high angles of attack, so that the possibility of stalling is minimized [1].

It is possible to improve the aerodynamics of an aircraft by trying various types of wing profiles. Richard Kline and Floyd Fogleman designed several staggered airfoils designed solely for paper airplanes in 1960. Richard Kline's goal was to create a paper airplane that could fly long distances and automatically increase altitude by countering wind resistance and turbulence. Thus, he achieved the stepped wing profile. Kline Fogleman profile structure can also be called stepped wing profile. Stepped wing profiles enable the creation of a vortex-shaped airflow by preventing the separation of the airflow and maintaining the airflow. The airflow behind the step is separated from the airfoil [1]. After making preliminary examinations and models, the designers submitted their patents to the patent office [2]. The NACA 0012 airfoil is a symmetrical wing profile without any humps, commonly employed in diverse aviation applications. Similar to the KFm-4 profile, it exhibits excellent performance at low Mach numbers. [3].

In the 21st century, the KF airfoil has seen renewed interest among radio-controlled aircraft enthusiasts due to its simplicity of construction, but it has not been adopted for full-size aircraft capable of carrying pilots, passengers or other significant payloads. Poor lift-to-drag ratio performance in wind tunnel tests means that to date the KF airfoil has not been used on any full-size aircraft. However, the KF airfoil and its derivative 'staggered' airfoils have gained a following in recent years in the world of radio-controlled model airplanes made of foam. Their low Reynolds numbers allow staggered airfoils to generate a significant amount of lift for the friction incurred, which has made them increasingly popular with RC enthusiasts. This paper investigates the advantages and disadvantages of choosing the KFm-4 airfoil over the NACA0012 airfoil due to its ease of manufacture, in comparison to the NACA0012 airfoil, which is generally preferred for high subsonic speeds.

In this study, k-ω SST turbulence model was used to simulate the problem using CFD analysis [4]. A comparison was made in terms of lift and drag coefficients of both airfoils at 0.6 Mach speed. Understanding low Reynolds number aerodynamics holds paramount importance in both military and civilian sectors. Consequently, this investigation places particular emphasis on examining the separation phenomena at the trailing edge of symmetrical airfoils operating within the constraints of low Reynolds numbers. [4].

2. Materials and Methods

2.1 Force Equations

Drag F_D and Lift F_L are basically expressed in two terms and these are dimensionless coefficients [5]:

Corresponding Author: Muktedir Gözüm
E-mail: muktedir.gozum@hotmail.com

$$C_D = \frac{F_D}{\frac{1}{2}\rho_\infty v_\infty{}^2 A} \qquad (1)$$

$$C_L = \frac{F_L}{\frac{1}{2}\rho_\infty v_\infty{}^2 A} \qquad (2)$$

The occurrence of lift in an airfoil depends on several factors such as air density, airflow velocity, angle of attack and total area of the airfoil. In the equation above, C_D and C_L are the drag and lift coefficients, F_D and F_L are the drag and lift forces, ρ_∞ is the density of the air, v_∞ is the cruise speed and A is the wing area.

2.2 Other Equations
Other equations used are listed here:

Continuity equation [5]:

$$\nabla.\vec{v} = 0 \qquad (3)$$

Conservation of momentum [5]:

$$\frac{\partial \vec{v}}{\partial t} + \vec{v}\nabla.\vec{v} = -\frac{1}{\rho}\nabla p + \frac{\mu}{\rho_0}\nabla^2\vec{v} + \vec{g} - \beta(T - T_0)\,\vec{g} \qquad (4)$$

β is the coefficient of thermal expansion. Conservation of Energy [5]:

$$\frac{\partial T}{\partial t} + \vec{v}.\nabla T = \alpha\nabla^2 T \qquad (5)$$

2.3 Turbulence Model
In the setup section, the solver type was selected as density based for compressible flow [5]. Air speed is taken into account as 0.6 Mach. The k-ω SST turbulence model was used to simulate the problem [6].

The specific dissipation rate of kinetic energy is solved by k-ω turbulent models. This model requires computers with higher memory for calculation. It is quite sensitive and difficult to converge. The equations for the models are below [6].

k-ε turbulence model equation [6]:

$$\frac{\partial}{\partial t}(\rho k) + \frac{\partial}{\partial x_i}(\rho k u_i) = \frac{\partial}{\partial x_j}\left[(\mu + \frac{\mu_t}{\sigma_k})\frac{\partial k}{\partial x_j}\right] + G_k + G_b - \rho\epsilon - Y_k + S_k \qquad (6)$$

$$\frac{\partial}{\partial t}(\rho\epsilon) + \frac{\partial}{\partial x_i}(\rho\epsilon u_i) = \frac{\partial}{\partial x_j}\left[(\mu + \frac{\mu_t}{\sigma_\epsilon})\frac{\partial\epsilon}{\partial x_j}\right] + C_{1\epsilon}\frac{\epsilon}{k}(G_k + C_{3\epsilon}G_b) - C_{2\epsilon}\rho\frac{\epsilon^2}{k} + S_\epsilon \qquad (7)$$

k-ω turbulence model equation [6]:

$$\frac{\partial}{\partial t}(\rho k) + \frac{\partial}{\partial x}(\rho k u_i) - \frac{\partial}{\partial x_i}(\Gamma_k\frac{\partial k}{\partial x_i}) + G_k - Y_k + S_k \qquad (8)$$

$$\frac{\partial}{\partial t}(\rho\,\omega) + \frac{\partial}{\partial x}(\rho\omega u_i) = \frac{\partial}{\partial x_i}(\Gamma_\omega\frac{\partial\omega}{\partial x_i}) + G_\omega - Y_\omega + S_\omega \qquad (9)$$

Explanations of the symbols used in the formulas are; (G_k: Production of turbulent kinetic energy due to mean velocity gradients, G_b: Turbulent kinetic energy production due to lift force, G_ω: ω represents the derivation, Y_M: Undulating expansion in compressible turbulence towards overall dissipation velocity, Y_k and Y_ω: Dispersion of k and ω due to

turbulence, Γ_k and Γ_ω: Effective diffusion of k and ω respectively, S_k and S_w: User-defined source terms).

2.4 Model, Mesh and Boundary Conditions
The calculation model and research methodology were created using ANSYS Fluent 19 software [7]. Here, a flow analysis was performed around NACA 0012 and KFm-4 airfoils with the following initial parameters (Table 1). The calculation domain is divided into finite volumes by the calculation model, as shown in Figures 1, 2 and 5. The mesh structure is concentrated in computational areas where there are large changes in the calculated parameters.

Table 1. Calculation conditions

Density (Air)	1.225 kg/m³
Wind speed	204.17 m/s (0.6 Mach)
Angle of Attack	0 (Degrees)
Chord Length	1.0 m
Temperature	293 K
Reference Pressure	101325 Pa

While boundary conditions are generally used up to 20c in the geometry section before making the C type mesh,[4], [8], [9] in this study it was drawn taking into account the 12.5 c (c: chord) dimension.
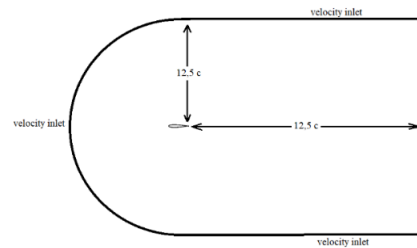

Figure 1. The computational domain around the airfoils

Chord length is taken into account as 1m. The inlet and walls are called fluid inlets, the exit part is called fluid outlet, and the wing boundaries are called airfoil [10].
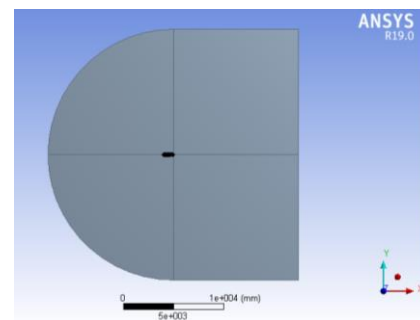

Figure 2. The computational domain around the airfoils in ANSYS for NACA 0012 and KFm-4
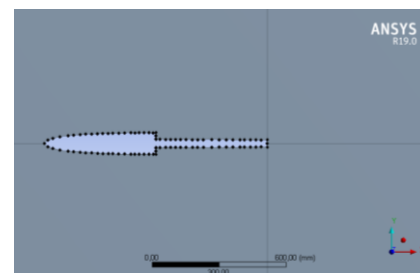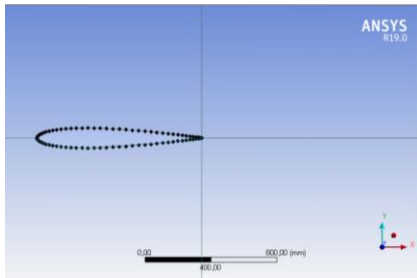

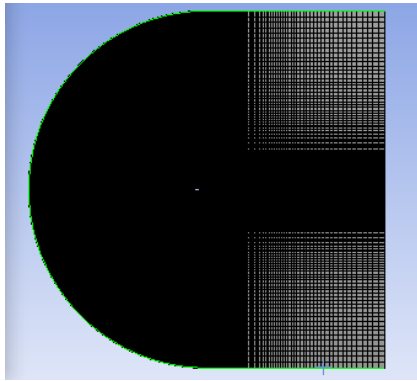**Figure 3.** KFm-4 Airfoil

Figure 4. NACA 0012 Airfoil

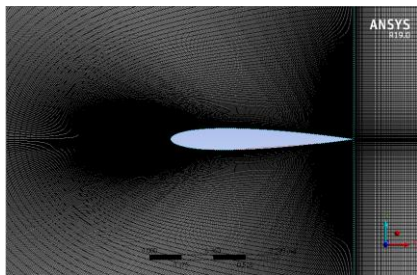**Figure 5.** Boundary condition and mesh structure for NACA 0012 (mapped mesh)

Figure 6. Mesh structure (mapped mesh)

Airfoil data on Ansys is shown as a drawing in Figures 3 and 4.

Table 2. Ansys mesh settings for NACA0012 and KFm-4 airfoils

Nodes	305100
Elements	303750
Mesh Metric	None
Suppressed	No
Type	Number of Divisions
Number of Divisions	450 225
Mapped Mesh	Yes
Method	Quadrilaterals
Constrain Boundary	No
Size Function	Uniform
Behavior	Hard
Bias Type	-------- ----- --- -
Bias Option	Bias Factor
Bias Factor	150.0

In the Table 2; Meshing process of KFm-4 Profile, 303750 meshes were cast (Number of elements). In Figure 6, the "Mapped Mesh" structure is shown on Ansys Fluent.

The freestream velocity is 204.17 m/s,
Density is 1.225 kg/m^3

Dynamic viscosity is 1.82e-5 kg/ms,
Boundary layer length is 1 m,
Y+ Value is 1,
Reynold number is 1.1e+6,
Estimated Wall distance is 2.0e-5.

3. Results and Discussion

As an initial condition, the airflow velocity is assumed to be equal to 204.17 m/s (0.6 Mach). The results of the numerical investigations are presented below. The distributions of the velocity field around the examined airfoil models and the pressure values for these models are shown (NACA 0012 and KFm-4). All figures are presented for 0-degree angle of attack. In Figure 7, the maximum dynamic pressure is shown as 83768 Pascal.
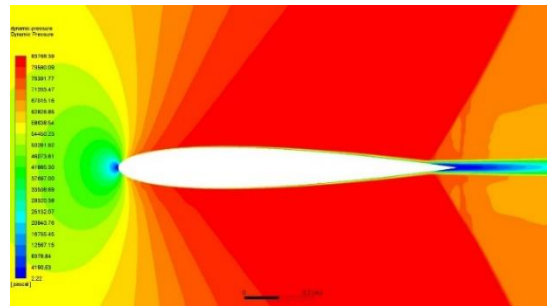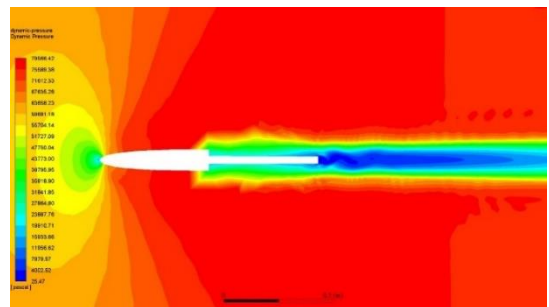

Figure 7. NACA 0012 dynamic pressure distribution (Pa)

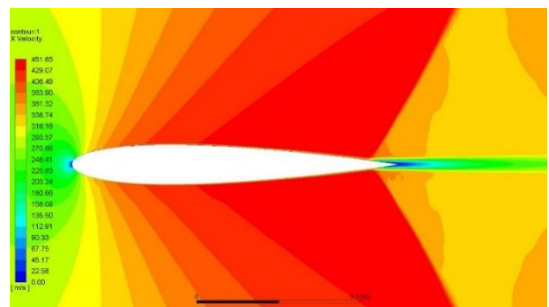**Figure 8.** KFm-4 Dynamic pressure distribution (Pa)

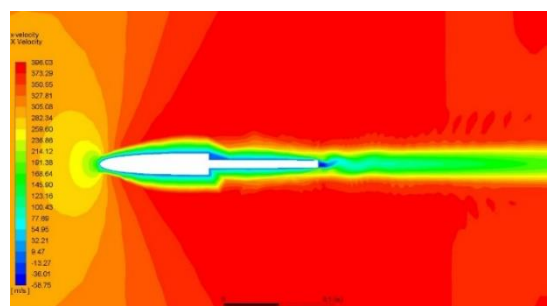**Figure 9.** NACA 0012 Speed distribution (m/s)

Figure 10. KFm-4 Speed distribution (m/s)

In Figure 8, the maximum dynamic pressure is shown as 79566.42 Pa. From the shapes of the pressure lines, it can be seen that the leading edge has lower pressure, while the upper and lower surfaces have higher pressure. This shows that the surfaces with high pressure try to lift the fuselage and therefore increase the lift coefficient, but it should not be forgotten that the analysis was carried out at 0-degree angle of attack and on a symmetrical airfoil. As can be seen from the figure, the pressure contours are distributed symmetrically and positioned to fully meet the wind (at 0 degrees). In the given form of pressure contours it is shown that there is a green color on the leading edge, on the lower and upper side the color is red, the red color indicates a higher-pressure value and the green color indicates a lower value.

As the angle of attack increases, the lift coefficient also increases, but when the angle of attack reaches 16 degrees, a stall situation will occur [6, 11].

In Figure 9, the maximum speed of the air flowing on the surface is shown as 451.65 m/s. The interpretation of Figure 9 is given in the conclusions section.

In Figure 10, the maximum speed of the air flowing on the surface is shown as 396.03 m/s. The interpretation of Figure 10 is given in the conclusions section.

When we look at the speed distributions above, we see that the highest speeds are reached as we move from the wing surface towards the tips. As you move towards the wing tips, the boundary layer becomes thinner, resulting in less drag and a higher speed at the wing tips. When we look at the speed distributions above, we see that the highest speeds are reached as we move from the wing surface towards the tips.

Table 3. Forces acting on NACA 0012 Profile

Lift	7165.5	N
Drag	-373.4	N
C_l	0.1010	
C_d	-0.0052	

Table 4. Forces acting on KFm-4 Profile

Lift	5109.40	N
Drag	-729.01	N
C_l	0.0720	
C_d	-0.0102	

The table 3 and 4 shows the force and coefficient values calculated as a result of the analysis. C_l, refers to the lift coefficient, and C_d refers to the drag coefficient. As can be seen from the table, at 0-degree angle, the NACA 0012 airfoil is superior to the KFm-4 profile in terms of lift and drag forces.

4. Conclusions

Aerodynamic comparison was made between the values assumed above and the results of modeling the flow in 2D. Special attention was paid to determine the 2D pressure distribution and velocity for the model with the initial parameters set. Based on the lift and drag forces in Table 3 and Table 4, it was concluded that the NACA 0012 airfoil was superior for 0 degrees.

In High Subsonic Speed Unmanned Aerial Vehicles, the KFm-4 airfoil can be used, but the NACA0012 airfoil is more suitable, especially when high subsonic speed is required. As a result of the analysis, it was seen that it is not suitable for use in large-sized and man-carrying aircraft compared to the NACA0012 profile.

However, KFm airfoils can increase the level of flight safety by reversing accidents that occur by exceeding critical angles of attack (stalling at higher angles). If these airfoils are designed in hybrid with NACA symmetric airfoils, they can provide a significant advantage. In a more detailed analysis, it is possible to formulate the following results:

- At high angles of attack, vortex formations can be seen on the upper surface of the airfoil.
- The results obtained in the analysis are based on numerical errors, the applicability of the computational models and the limitations of the mesh. For this reason, experimental verification of the numerical results should be performed on platforms such as wind tunnels.

Author contributions

Muktedir Gözüm: Research, Methodology, Design, Analysis and writing the original draft.

Cevat Özarpa: Formal analysis, Funding acquisition, Project management, Validation, Review and editing of the article.

References

1. Kowaleczko, G., Stryczniewicz, W., Szczepaniak, R., Bąbel, R., and Grzywacz, A., The effect of using the Kline-Fogleman modification upon the coefficient characteristics of aerodynamic forces in the airfoil, Journal of KONES Powertrain and Transport, **2018**, 25(2): 349–356
2. Fogleman, F., Kline, R., Airfoil for aircraft having improved lift generating device, US patent No. US4046338A, United States Patent and Trademark Office, **1977**
3. Fincham, J.H., and Friswell, M.I., Aerodynamic optimisation of a camber morphing aerofoil, Aerosp. Technol., **2015**, 43, 245–255
4. Lei, J., Guo, F., and Huang, C., Numerical study of separation on the trailing edge of a symmetrical airfoil at a low Reynolds number, Chinese J. Aeronaut., **2013**, 26(4): 918–925,
5. Kabir, M.A., Islam, M., Akib, Y.M., and Hafiz, A., Comparison between two Kline–Fogleman modified (KFm) based stepped airfoils for better aerodynamic performance, International Conference on Innovation in Engineering and Technology, Dhaka, Bangladesh, **2019**
6. Saraf, A.K., Singh, M.P., Chouhan T.J., Aerodynamic analysis of NACA 0012 airfoil using CFD, International Journal of Mechanical and Production Engineering, **2017**, 5(12): 21-25
7. ANSYS Inc., ANSYS Fluent Tutorial Guide 18, **2018**, 229-265
8. Z., Li, P., Zhang, T., Pan, and Q., Li, Study on effects of thickness on airfoil-stall at low Reynolds numbers by cusp-

catastrophic model based on GA (W) -1 airfoil, Chinese J. Aeronaut., **2020**, 33(5): 1444–1453

9. Zhen, T.K., Zubair, M., and Ahmad, K.A., Experimental and Numerical Investigation of the Effects of Passive Vortex Generators on Aludra UAV Performance, Chinese J. Aeronaut., 2011, 24(5): 577–583

10. Soğukpınar, H., Uçak Kanatlarinda En İdeal Hücum Açisini Bulmak İçin 4 Rakamli Naca 00xx Kanat Profillerinin Nümerik Analizi, Uludağ Üniversitesi Mühendislik Fakültesi Dergisi, **2017**, 22(1), 169-178

11. Simons, M., Model Aircraft Aerodynamics, 4 th., Adelaide: Argus Books, **1994**